The subtle effects of iron-containing metal surfaces on the reductive carbonylation of $RuCl_3$†

Matti Haukka,* Minna Jakonen, Taina Nivajärvi and Mirja Kallinen

Received 24th February 2006, Accepted 4th May 2006
First published as an Advance Article on the web 12th May 2006
DOI: 10.1039/b602834a

The use of iron-containing metal surfaces, Fe, Fe–Cr-alloy and stainless steel, for the synthesis of mixed metal Ru–Fe compounds has been studied. The studied process was reductive carbonylation of $RuCl_3$ in the presence of a metal surface. Reactions were carried out in ethanol solutions under 10–50 bar carbon monoxide pressure at 125 °C using an autoclave. During the reaction the metal surface was oxidized, releasing iron into the solution and acting as a sacrificial source of iron. Under these conditions the corrosion of the metal surface was facile and produced a series of iron-containing species. In addition to the formation of most obvious iron(II) products, such as $[Fe(H_2O)_6]^{2+}$ or $[FeCl_2(H_2O)_4]$ the use of the metal surface also provided a route to novel labile trinuclear $[Ru_2Cl_2(\mu\text{-}Cl)_4(CO)_6FeL_2]$ (L = H_2O, EtOH) complexes. The stability and reactivity of the $[Ru_2Cl_2(\mu\text{-}Cl)_4(CO)_6FeL_2]$ complexes were further studied using computational DFT methods. Based on the computational results a reaction route has been suggested for the formation and decomposition of $[Ru_2Cl_2(\mu\text{-}Cl)_4(CO)_6FeL_2]$.

1. Introduction

A solid metal surface can be involved in chemical reactions in various ways. A metallic material can serve as a redox agent or catalyst, facilitating a reaction, or it can release metal species into the system. The metal can be released as oxidized products *via* corrosion processes or, in some cases, even as formally zerovalent compounds. As a well-known example, $Fe(CO)_5$, and especially $Ni(CO)_4$, can be obtained by the direct interaction between CO and the metal. The controlled release of metal species from a surface has been exploited in several chemical, biochemical and synthetic chemistry processes. It has long been known that, for example, under catalytic reaction conditions the walls of the metallic reaction vessels can have an influence on the reaction.[1] The released metal can even promote the catalysis processes. However, in these processes the release of the metal is usually not well controlled, and often the released metal compounds are not completely characterized. The most common method of taking advantage of controlled metal release from a bulk metal is to use sacrificial electrodes. Sacrificial electrodes have been applied, for example, to control the iron concentration in the feed water of nuclear boiling water reactors,[2] to release ions into the water as a biocide[3] or for electroflocculation in order to provide a coagulating agent for the waste water.[4,5] The electrochemical synthesis of tetramethyl lead and some other organometallic compounds was patented as long ago as the mid-1960s,[6] while the electrosynthesis of functionalized 2-arylpyridines,[7] functionalized organozinc compounds[8] and also the aminopyridine derivatives of Co, Ni, Zn, and Cu[9] are more recent examples of the successful use of sacrificial electrodes in synthetic chemistry.

The primary objective of the present work was to apply the sacrificial surface approach to the synthesis of mixed metal Ru–Fe–Ru carbonyl compounds. The studied process was carbonylative reduction of $RuCl_3$ in the presence of an iron-containing metal surface. Ruthenium carbonyls are most commonly synthesized by reducing $RuCl_3$ under a CO atmosphere.[10–18] The pioneering work in this area was accomplished by Chatt and co-workers in the mid 1960's.[10] These reactions are typically carried out in an alcoholic solution,[10–19] either under elevated CO pressure or under reflux in a flow of CO.[10–15,17,18] Zerovalent ruthenium carbonyl clusters have also been synthesized by CO reduction of $[RuCl_2(CO)_3]_2$ in the presence of alkalicarbonyls.[20] Several methods, quite different both mechanistically and in terms of efficiency, have been suggested to improve the reduction of ruthenium chlorides or carbonyl chlorides: for example, reduction in the presence of Zn,[12] hydroxide ions[13,14,21,22] or carbonates.[23] Silver acetate has also been reported to be useful in enhancing the reduction of ruthenium halides.[24] Another approach that has been used to improve the reduction is to use the surfaces to assist the reduction. Surface-mediated carbon monoxide reductions of ruthenium halides have been carried out primarily on oxide surfaces.[25–28]

In the present study the carbonylative reduction of ruthenium chloride was carried out in an alcoholic solution in the presence of iron-containing metal surfaces: iron, stainless steel or Fe–Cr-alloy. The goal was to take advantage of the iron released from the surface during the process. The effect of the reaction conditions on this process is discussed. The product distribution was analyzed, and the formation and stability of the new mixed metal products $[Ru_2Cl_2(\mu\text{-}Cl)_4(CO)_6FeL_2]$ (L = H_2O, EtOH) were further investigated by means of DFT calculations. Based on these results a reaction route for the decomposition of $[Ru_2Cl_2(\mu\text{-}Cl)_4(CO)_6FeL_2]$ (L = H_2O, EtOH) is also suggested.

Department of Chemistry, University of Joensuu, Department of Chemistry, P.O. Box 111, FI-80101, Joensuu, Finland. E-mail: matti.haukka@joensuu.fi; Fax: +358-13-251 3390

† Electronic supplementary information (ESI) available: Thermal ellipsoid plots (at 50 % probability level) of **1b**, **1c**, **2**, and **3**. See DOI: 10.1039/b602834a

2. Experimental

2.1. Materials

Ethanol (Primalco, 99.9%) and $RuCl_3 \cdot n(H_2O)$ (Alfa Aesar, p.a.) were used without further purification. Carbon monoxide (99.999%) was obtained from Aga. Metal plates: Iron (Fe) foil (thickness: 0.25 mm, purity 99.5%, product number: FE000400/11), stainless steel-17-7PH (thickness 0.3 mm, 76% Fe, 17% Cr and 7% Ni, product number: FE280350/2), Fe–Cr-alloy® (iron/chromium) (thickness 1.0 mm 72.8% Fe, 22% Cr, 5% Al, 0.1% Y and 0.1% Zr, product number: FE080600/4) plates were purchased from Goodfellow. Iron powder was obtained from Merck.

2.2. Reactions

The reactions at low pressures under a CO flow were performed in a round-bottom, two-neck flask. Carbon monoxide was introduced into the system by bubbling the gas through the solution. In a typical reaction, a 250 mg sample of $RuCl_3 \cdot n(H_2O)$, 40 ml of ethanol and *ca.* 100 mg of the metallic component (metal plates or powder) were placed in the bottom of the reaction vessel. The solution was heated under reflux overnight (17–20 h), after which it was cooled to room temperature and filtered. The solution was then evaporated to dryness for further analysis. Low-pressure reactions with different metal plates were repeated under these conditions *ca.* 10–20 times. The total yield of solid products were *ca.* 200–230 mg. The crystals for X-ray analysis either were obtained directly from the reaction solution or the dried product was dissolved in CH_2Cl_2 and crystallized by adding hexane to the dichloromethane solution.

All of the high-pressure (≥10 bar) syntheses were carried out in a 10 mL Berghof Autoclave equipped with a PTFE liner. In a typical experiment, a 100 mg sample of $RuCl_3 \cdot n(H_2O)$ was introduced into the autoclave with 4 mL of solvent (ethanol or water) and one to three metal plates (total weight: 50–100 mg, size of the plates: 7 × 7 × 0.3–1.0 mm). The reactions were performed using iron, stainless steel, and Fe–Cr-alloy under 10, 20 and 50 bar of CO at 125 °C. The reaction times were 1, 3, 6, 17 and 20 h. Each reaction was repeated several times. After each reaction the autoclave was cooled down in an ice bath. The solid products were filtered off and the resulting solution was evaporated to dryness. The total yield of solid products was *ca.* 100–120 mg. The crystals for X-ray analysis were obtained directly from the ethanol solution during slow evaporation, or by crystallization from dichloromethane solution.

In ethanol at 50 bar CO pressures and longer reaction times (>3 h) the main product was $Ru_3(CO)_{12}$ (yield *ca.* 80% after 17 h reaction). $Ru_3(CO)_{12}$ was partially precipitated as an orange solid during the reaction and the remainder was recovered by evaporating the solution to dryness. In longer (>3 h) reactions at 50 bar CO pressure, variable amounts of $[RuCl_2(CO)_3]_2$ were also formed, but this was always a minor product. When the reaction was conducted in water, the final carbonylation product was polymeric $[Ru(CO)_4]_n$, which was also obtained in high yield (75–80%, after 17 h reaction). These known products[15,29,30] were identified by IR, elemental analysis, and X-ray diffraction techniques (single crystal or powder diffraction).

In ethanol at lower CO pressures (20 bar) and shorter reaction times (≤3 h) the product did not contain any solid material. Only minor amounts of zerovalent ruthenium carbonyls or $[RuCl_2(CO)_3]_2$ were found, or none at all. The main components, colorless $[RuCl_3(CO)_3]_2[Fe(H_2O)_6]$ and the yellowish trinuclear $[Ru_2Cl_2(\mu\text{-}Cl)_4(CO)_6FeL_2]$ (L = H_2O, EtOH), were separated mechanically after crystallization and analyzed by IR, elemental analysis and single-crystal X-ray diffraction. Other minor species, $RuCl_2(H_2O)(CO)_3$, $FeCl_2(H_2O)_4$, and $[RuCl_3(CO)_3][Fe(H_2O)_6]$, which were found in some reaction products, were characterized only by single-crystal X-ray diffraction.

The individual yields of $[RuCl_3(CO)_3]_2[Fe(H_2O)_6]$, $[Ru_2Cl_2(\mu\text{-}Cl)_4(CO)_6FeL_2]$ (L = H_2O, EtOH), $RuCl_2(H_2O)(CO)_3$, $FeCl_2(H_2O)_4$, or $[RuCl_3(CO)_3][Fe(H_2O)_6]$ are not reported here since the reaction products were typically mixtures of the above species with variable ratios. The ratio varied even when the reactions were repeated using the same reaction conditions.

Analysis of products 1, 4, and 5.

*$[Ru(CO)_3Cl_3]_2[Fe(H_2O)_6]$ (**1**).* IR ν(CO) (in CH_2Cl_2): 2141 (vs) cm^{-1}, 2074 (vs) cm^{-1}; ν(CO) (in KBr): 2143 (s) cm^{-1}, 2074 (sh) cm^{-1}, 2060 (vs, br) cm^{-1}. Calcd.: C 9.65%, H 1.62%, Found: C 9.68%, H 1.56%.

*$[Ru_2Cl_2(\mu\text{-}Cl)_4(CO)_6Fe(CH_3CH_2OH)_2]$ (**4**).* IR ν(CO) (in CH_2Cl_2): 2143 (vs) cm^{-1}, 2076 (vs) cm^{-1}. Calcd.: C 16.43%, H 1.65%, Found: C 16.34%, H 1.81%.

*$[Ru_2Cl_2(\mu\text{-}Cl)_4(CO)_6Fe(H_2O)_2]$ (**5**).* IR ν(CO) (in KBr): 2149 (s), broad signal at *ca.* 2075 (vs) cm^{-1} or double-headed signal at 2079 (vs) cm^{-1} and 2071 (vs) cm^{-1}. IR ν(CO) (in CH_2Cl_2): 2142 (vs) cm^{-1}, 2075 (vs) cm^{-1}. No distinction could be made between the linear and the bent isomers of **5**. Calcd. for $[Ru_2Cl_2(\mu\text{-}Cl)_4(CO)_6Fe(H_2O)_2] \cdot 2(H_2O)$: C 10.14%, H 1.13%, Found: C 10.04%, H 1.38%.

2.3 X-Ray crystal structure determinations

The crystals were immersed in cryo-oil, mounted in a Nylon loop and measured at a temperature of 100 K or 120 K. The X-ray diffraction data were collected by means of a Nonius KappaCCD diffractometer using Mo-Kα radiation (λ = 0.71073 Å). The Denzo-Scalepack program package[31] was used for cell refinements and data reductions. All of the structures were solved by direct methods using the SHELXS97, SIR2004, or SIR97[32–34] with the WinGX graphical user interface.[35] An empirical absorption correction was applied to all of the data (XPREP in SHELXTL v.6.14-1).[36] Structural refinements were carried out using SHELXL97.[37] Both H_2O and OH hydrogens were located from the difference Fourier map in all structures. The H_2O hydrogens were located from the difference Fourier and restrained to ride on their parent atom (U_{iso} = 1.5 U_{eq} (parent atom)) using the observed O–H distance or refined with a restrained O–H distance (0.85 Å). All other hydrogens were placed in idealized positions and constrained to ride on their parent atom. The crystallographic details are summarized in Table 1. The selected bond lengths and angles are shown in Table 2. The structures of **2** and **3** are known and have been published previously by others.[38–41]

CCDC reference numbers 299525–299534.

For crystallographic data in CIF or other electronic format see DOI: 10.1039/b602834a

Table 1 Crystallographic data for **1**, **1b**, **1c**, **2**, **3**, **4**, **5**, **5b**, **5c**, and **6**

	1	**1b**	**1c**	**2**	**3**	**4**	**5**	**5b**	**5c**	**6**
Empirical formula	$C_6H_{12}Cl_6FeO_{12}Ru_2$	$C_6H_{16}Cl_6FeO_{14}Ru_2$	$C_6H_{16}Cl_6FeO_{14}Ru_2$	$Cl_2FeH_8O_4$	$C_3H_2Cl_2O_4Ru$	$C_{10}H_{12}Cl_6FeO_8Ru_2$	$C_6H_4Cl_6FeO_8Ru_2$	$C_6H_6Cl_6FeO_9Ru_2$	$C_6H_4Cl_6FeO_8Ru_2$	$C_3H_{12}Cl_3FeO_9Ru$
M	746.85	782.88	782.88	198.81	274.02	730.89	674.78	692.80	674.78	526.30
T/K	100(2)	150(2)	100(2)	120(2)	120(2)	120(2)	120(2)	120(2)	140(2)	120(2)
λ/Å	0.71073	0.71073	0.71073	0.71073	0.71073	0.71073	0.71073	0.71069	0.71073	0.71073
Crystal system	Triclinic	Triclinic	Triclinic	Monoclinic	Monoclinic	Monoclinic	Monoclinic	Triclinic	Monoclinic	Monoclinic
Space group	$P\bar{1}$	$P\bar{1}$	$P\bar{1}$	$P2_1/n$	$P2_1/n$	$P2_1/c$	$P2_1/n$	$P\bar{1}$	$P2_1/c$	$P2_1/n$
a/Å	6.2958(6)	6.2478(5)	6.2244(1)	5.8738(3)	6.2164(3)	9.2270(7)	7.0444(4)	6.9100(2)	10.1193(2)	11.7975(5)
b/Å	6.4156(4)	7.1825(7)	13.0253(2)	7.1006(5)	10.2373(5)	10.9769(6)	15.6274(3)	11.7730(5)	6.4008(1)	9.4944(2)
c/Å	13.9122(14)	14.7889(16)	15.4469(4)	8.4040(4)	11.7124(5)	11.0272(8)	8.5003(7)	12.5560(5)	27.7787(8)	15.1011(6)
α/°	87.513(5)	92.023(4)	70.985(1)	90	90	90	90	103.407(2)	90	90
β/°	77.295(4)	97.730(4)	85.508(1)	109.623(3)	97.922(3)	96.796(4)	97.016(3)	101.573(2)	95.3390(9)	107.635(2)
γ/°	80.322(6)	115.042(5)	89.077(1)	90	90	90	90	95.605(2)	90	90
V/Å^3	540.36(8)	592.65(10)	1180.32(4)	330.15(3)	738.25(6)	1109.03(13)	928.75(9)	962.20(6)	1791.47(7)	1611.99(10)
Z	1	1	2	2	4	2	2	2	4	4
ρ_{calc}/Mg m^{-3}	2.295	2.194	2.203	2.000	2.465	2.189	2.413	2.391	2.502	2.169
μ(Mo-Kα)/mm^{-1}	2.832	2.594	2.605	3.017	2.797	2.745	3.267	3.160	3.387	2.693
$R1^a$ ($I \geq 2\sigma$)	0.0412	0.0321	0.0234	0.0214	0.0219	0.0308	0.0253	0.0300	0.0242	0.0251
$wR2^b$ ($I \geq 2\sigma$)	0.0758	0.0857	0.0605	0.0509	0.0436	0.0619	0.0596	0.0616	0.0578	0.0567

^{a} $R1 = \sum ||F_o| - |F_c|| / \sum |F_o|$. ^{b} $wR2 = [\sum[w(F_o^2 - F_c^2)^2] / \sum[w(F_o^2)^2]]^{1/2}$.

2.4 Computational work

The full geometry optimization of the structures was conducted by using the non-local hybrid density functional method B3PW91, as implemented in the Gaussian03 program.[42] The basis set was the standard 6-31G* for all elements except Ru and Fe, for which the Stuttgart–Dresden ECP basis set was used.[43] In the case of ruthenium, the ECP basis set was augmented by a p-type polarization function with an exponent of 0.086.[44] The Hessian matrix was calculated analytically for all structures in order to verify the location of the global minima (none of the optimized structures had imaginary frequencies).

3. Results and discussion

3.1 Reductive carbonylation of $RuCl_3$ in the presence of a sacrificial metal surface

When $RuCl_3$ is reduced by carbon monoxide in an alcoholic solution, the originally dark solution first turns into a "ruthenium red carbonyl solution".[10,11] If the reaction is continued, a yellow solution is obtained. Mantovani and Cenini reported that the reduction at low pressures produces a lemon-yellow solution of uncharacterized ruthenium carbonyl chloride $Ru(CO)_nCl_m$.[12] When the reaction was repeated in the presence of an iron-containing metal surface it followed the same steps. Under reflux and in a stream of carbon monoxide the reaction solution first turned slowly from black to dark red and finally to yellow or greenish yellow. At this point a sample of the solution was dried, dissolved in dichloromethane and analyzed using IR spectroscopy. The IR spectrum typically showed a simple pattern of two strong ν(CO) frequencies at *ca.* 2141 cm^{-1}and 2074 cm^{-1} (in CH_2Cl_2). The pattern resembles the spectrum of the $[RuCl_2(CO)_3]_2$ dimer (2144 cm^{-1}and 2083 cm^{-1} in CH_2Cl_2), but the bands are shifted towards lower wavenumbers. The higher frequency band at 2141 cm^{-1} was sharp and the lower band broader or double headed. This type of pattern is typical of a symmetrical octahedral ruthenium tricarbonyl species of the type $[RuX_3(CO)_3]$ with facially arranged carbonyls.[45] The spectrum could be assigned to $[RuCl_3(CO)_3]^-$ ions. However, when the reactions were repeated several times some variation was observed in the spectra, indicating that the process was not completely repeatable. Both the wavenumbers and the number of carbonyl signals and also their relative intensities varied, suggesting the presence of more than one metal carbonyl species with variable ratios. Nevertheless, the reaction followed a similar path in all reactions. In all cases, the metal surface was roughened and corroded. The wearing-out of the metal surface indicates that it had been involved in redox reaction and had released iron into the solution. The nature of the corrosion was found to be dependent on the solid material. Stainless steel tended to undergo typical pitting corrosion, while the pure iron and Fe–Cr-alloy surfaces were worn more uniformly. In some reactions a blackish powdery material, rich in Ru, accumulated on the metal surface. The amount of the blackish powder was also dependent on the metal surface used, occurring especially in reactions with stainless steel. The formation of a solid blackish side product of RuO_2 during the high pressure reductive carbonylation of $RuCl_3$ had been reported earlier by Bruce *et al.*[19] Thus, RuO_2 could also be formed in our

Table 2 Selected bond lengths (Å) and angles (°) for **1**, **4**, **5**, **5b**, **5c**, and **6**

	1	**4**	**5**	**5b**	**5c**	**6**
Ru1–Cl1	2.4166(12)	2.4178(8)	2.4145(8)	2.4316(9)	2.4125(9)	2.4281(6)
Ru1–Cl2	2.4162(14)	2.4224(8)	2.4350(7)	2.4275(9)	2.4273(9)	2.4173(6)
Ru1–Cl3	2.4102(13)	2.4176(8)	2.4182(9)	2.4073(9)	2.3974(9)	2.4220(6)
Ru1–C1	1.910(6)	1.895(4)	1.907(3)	1.898(4)	1.914(4)	1.907(3)
Ru1–C2	1.892(6)	1.907(4)	1.915(3)	1.914(4)	1.921(4)	1.918(2)
Ru1–C3	1.937(6)	1.905(3)	1.918(4)	1.930(4)	1.919(4)	1.898(3)
Fe1–O4	2.153(3)	2.043(2)	2.089(2)			2.0702(17)
Fe1–O5	2.102(4)					2.0571(16)
Fe1–O6	2.111(4)					2.0680(17)
Fe1–O7					2.070(3)	2.0069(17)
Fe1–O8					2.146(3)	
Fe1–Cl1		2.5132(8)	2.5036(7)	2.4935(9)	2.5145(10)	
Fe1–Cl2		2.5415(8)	2.4624(7)	2.5000(10)	2.4573(10)	
Fe1–Cl4				2.5287(9)	2.4994(10)	2.2501(7)
Fe1–Cl5				2.4912(9)	2.4681(10)	2.3038(6)
Ru2–Cl4				2.4210(9)	2.4201(9)	
Ru2–Cl5				2.4164(8)	2.4243(9)	
Ru2–Cl6				2.4236(9)	2.3990(10)	
Ru2–C4				1.916(4)	1.899(4)	
Ru2–C5				1.907(4)	1.900(4)	
Ru2–C6				1.915(4)	1.922(4)	
Cl1–Ru1–Cl2	89.36(5)	90.69(10)	90.46(9)	86.83(3)	86.83(3)	88.97(2)
Cl1–Ru1–Cl3	89.12(4)	90.23(3)	89.85(3)	91.20(3)	87.79(3)	89.94(2)
C1–Ru1–C2	92.6(2)	91.65(14)	91.14(13)	89.65(15)	93.03(15)	92.98(10)
C1–Ru1–C3	92.0(2)	91.38(13)	92.63(13)	92.08(14)	93.92(15)	88.54(10)
O4–Fe1–O5	88.99(14)					81.28(6)
O4–Fe–O6	90.61(13)					88.64(7)
Cl1–Fe1–Cl2A		98.93(3)	96.07(2)			
O7–Fe1–O8				87.21(10)	87.79(11)	
Cl1–Fe1–Cl4				169.75(3)	173.77(4)	
Cl2–Fe1–Cl5				93.11(3)	90.08(3)	
Cl4–Fe1–Cl5				81.96(3)	84.91(3)	97.74(2)
Cl6–Ru2–Cl4				90.33(3)	89.02(3)	
Cl6–Ru2–Cl5				89.14(3)	87.41(3)	
C6–Ru2–C4				91.66(15)	91.85(16)	
C6–Ru2–C5				92.12(14)	91.43(16)	

system. Nevertheless, a possible formation of metallic Ru cannot be completely ruled out. Although the metal surface was clearly corroded, no iron-oxo species were observed. The formation of the blackish layer hindered the reductive carbonylation of $RuCl_3$. If the same metal particles were used again in a reaction without the surface having been cleaned, the yellow solution took considerably longer to form. Such results suggest that the metal surface also takes part in the reduction of $RuCl_3$.

To facilitate an investigation in to the role of the metal surface and the effect of the reaction conditions, the carbonylation of $RuCl_3$ in the presence of a plate, was repeated in an autoclave (equipped with a Teflon liner) at an elevated temperature (125 °C) under variable CO pressures (10–50 bar) using different reaction times (1–24 h). Each reaction was repeated several times in order to see whether the product distribution obtained under certain conditions was reproducible. Again, the metal surfaces were clearly corroded in all reactions (Fig. 1). Compared with heating under reflux in a CO stream, the use of an autoclave and high pressures accelerated and enhanced the carbonylation. As a result of the more efficient carbonylation conditions, the zerovalent $Ru_3(CO)_{12}$ was typically the dominant final reduction product at high pressures of CO (50 bar), although at least traces of $[RuCl_2(CO)_3]_2$ could also be found even after 20 h of reaction. Both of these products crystallized directly from the reaction solution and were identified by IR and single-crystal X-ray diffraction. As might be expected, the formation of the $Ru_3(CO)_{12}$ was favored by the longer reaction times. Similarly, the formation of the blackish, powdery, inactivating layer on the metal surface was favored by long reaction times and high pressures. The solvent was found to have a strong effect on the final carbonyl product. We have previously reported that the reduction of $RuCl_3$ under 50 bar of CO

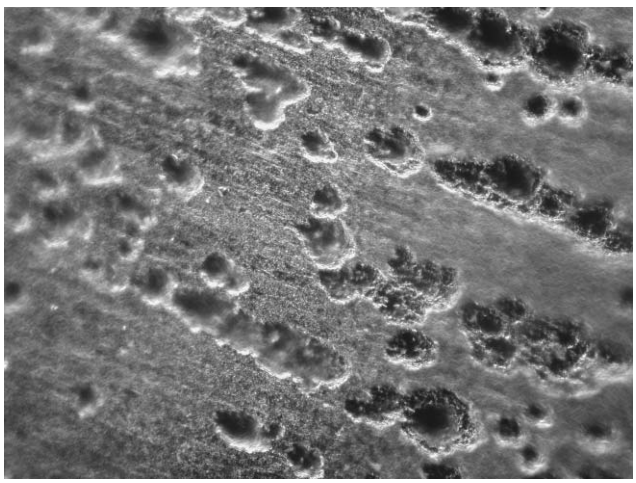

Fig. 1 Pitting corrosion on a stainless steel surface after 3 h of reaction at 50 bar of CO (under × 500 magnification).

in water produces polymeric $[Ru(CO)_4]_n$ instead of $Ru_3(CO)_{12}$.[30] A similar solvent effect was also observed in reductions with metal surfaces. In water the polymeric $[Ru(CO)_4]_n$ replaced $Ru_3(CO)_{12}$ as the dominant final carbonylation product.

At lower CO pressures (20 bar) the formation of $Ru_3(CO)_{12}$ and $[RuCl_2(CO)_3]_2$ was strongly suppressed. After a three-hour reaction at 125 °C at 10 bar CO pressure, a yellow solution was obtained, but no significant formation of $Ru(CO)_{12}$ or $[RuCl_2(CO)_3]_2$ could be observed. The yellow solution was evaporated to dryness and the resulting solid product was dissolved in CH_2Cl_2 and crystallized by adding hexane slowly to the dichloromethane solution. Typically, the final precipitate contained a colorless crystalline material as the main product, with some larger yellowish crystals. Both materials were analyzed by means of single-crystal X-ray crystallography. The colorless product was identified as ionic $[RuCl_3(CO)_3]_2[Fe(H_2O)_6]$ (**1**) with Ru and Fe in oxidation state +2 (Fig. 2).

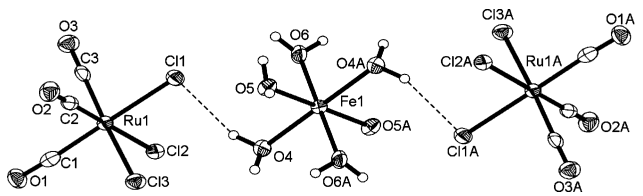

Fig. 2 Thermal ellipsoid plot of $[RuCl_3(CO)_3]_2[Fe(H_2O)_6]$ (**1**). The ellipsoids have been drawn at 50% probability level. The Ru and Fe moieties are held together by weak hydrogen bonding interactions. For example: O4–H4A: 0.92 Å, H4A···Cl1: 2.34 Å, O4···Cl1: 3.186(4) Å, Ru1–H4A···Cl1: 154.5° (symmetry transformations used to generate equivalent atoms: A: $1-x$, $1-y$, $1-z$).

In some cases **1** was crystallized in other crystal systems with water of crystallization as $[RuCl_3(CO)_3]_2[Fe(H_2O)]\cdot 2(H_2O)$ (structures **1b** and **1c**). Structurally, $[RuCl_3(CO)_3]_2[Fe(H_2O)_6]$ is isomorhphous with $[RuCl_3(CO)_3]_2[Ru(H_2O)_6]$.[41] Although formation of $[RuCl_3(CO)_3]_2[Ru(H_2O)_6]$ could be possible also during the reduction of $RuCl_3$ with metal surfaces no evidence of this was observed. X-Ray analysis of a series of crystalline products showed only the presence of mixed metal **1**, where the ruthenium and iron units are held together by weak hydrogen bonds. Although $[RuCl_3(CO)_3]_2[Fe(H_2O)_6]$ was obtained after only short reaction times and with relatively low pressures, some traces of it were found even after 20 h of reaction under 50 bar of CO. An additional aqueous iron species $FeCl_2\cdot 4(H_2O)$, which can also be seen as *trans*(Cl)-$[FeCl_2(H_2O)_4]$ (**2**), was also found in some reaction products obtained at 20 bar of CO, 3 h reaction time and 125 °C using an iron plate. It was only a minor product and was not observed at all in most of the reactions. The structure of **2** was verified by means of single-crystal X-ray diffraction. The presence of aqueous iron species was unsurprising, since the formation of such moieties can be expected as a consequence of the corrosion process of an iron-containing metal surface. Even if the reaction is carried out in ethanol (99.9%) water is nevertheless available. Water is introduced to the system by the solvent as well as by the $RuCl_3\cdot n(H_2O)$. Furthermore, although the metal plates were washed with ethanol prior to use, they can also be a source of water. In addition to iron, partially reduced ruthenium also produced the neutral mononuclear aqua complex $RuCl_2(H_2O)(CO)_3$ (**3**) as a minor side-product in some of the high pressure reactions performed at 20 bar of CO, 3 h reaction time and 125 °C using an iron plate. Like *trans*(Cl)-$[FeCl_2(H_2O)_4]$ this product was strictly a minor product, which was not found at all in most of the reactions.

The second component found in the reaction product, a yellowish crystalline material, was typically a mixture that contained two types of complex in a variable ratio: $[Ru_2Cl_2(\mu\text{-}Cl)_4(CO)_6Fe(CH_3CH_2OH)_2]$ (**4**) and $[Ru_2Cl_2(\mu\text{-}Cl)_4(CO)_6Fe(H_2O)_2]$ (**5**). Both of these species were characterized crystallographically (Fig. 3 and 4). The formation of complexes **4** and **5** was somewhat more surprising than the formation of complexes **1–3**, since trinuclear halide-bridged ruthenium compounds are relatively rare. To our knowledge, the only other known example of linear Ru–(μ-Cl)$_2$–M–(μ-Cl)$_2$–Ru mixed metal systems is $[\{cis\text{-}RuCl_2(dppm)_2\}_2Cu]^+$.[46] In addition to this, a few linear homometallic trinuclear ruthenium compounds of the type Ru–(μ-Cl)$_3$–Ru–(μ-Cl)$_3$–Ru with three chloride bridges are also known to exist.[47–51]

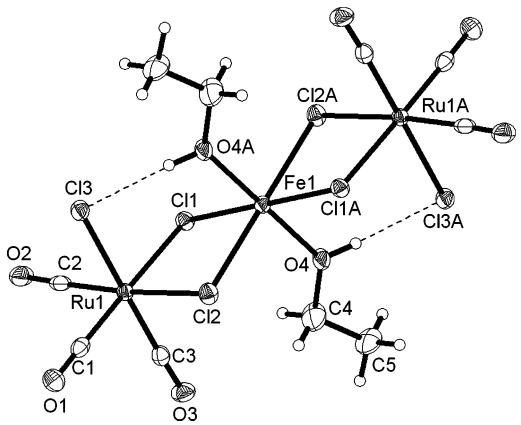

Fig. 3 Thermal ellipsoid plot of $[Ru_2Cl_2(\mu\text{-}Cl)_4(CO)_6Fe(CH_3CH_2OH)_2]$ (**4**). The ellipsoids have been drawn at 50% probability level. Intramolecular hydrogen bonding interactions: O4–H4: 0.85 Å, H4···Cl3A: 2.25(2) Å, O4···Cl3A: 3.073(3) Å, O4–H4···Cl3A: 162° (symmetry transformation used to generate equivalent atoms: A: $-x+1$, $-y$, $-z+1$).

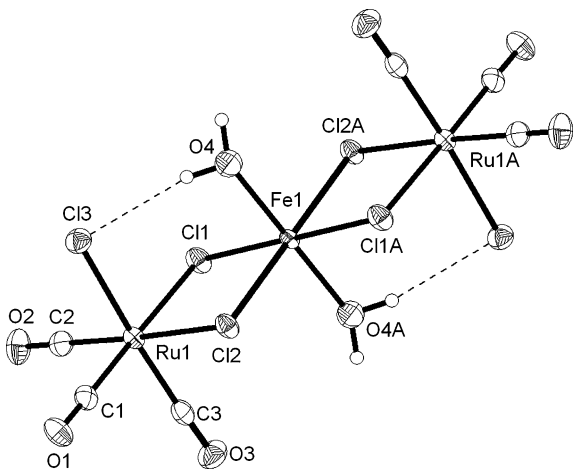

Fig. 4 Thermal ellipsoid plot of the linear $[Ru_2Cl_2(\mu\text{-}Cl)_4(CO)_6Fe(H_2O)_2]$ (**5**). The ellipsoids have been drawn at 50% probability level. Intramolecular hydrogen bonding interactions: O4–H4B: 0.85 Å, H4B···Cl3: 2.457(10) Å, O4···Cl3: 3.293(2) Å, O4–H4···Cl3: 168° (symmetry transformation was used to generate equivalent atoms A: $1-x$, $-y$, $-z$).

Complex **4** was typically the dominant trinuclear product in low pressure reactions (10 bar) and the amount of **5** tended to increase with increasing pressure. However, traces of complex **5** were also found in the low pressure reactions. Structurally, compound **4** contains two Ru centers and an iron center in the oxidation state +2. The linear trinuclear Ru–Fe–Ru architecture is supported by intramolecular hydrogen bonds between the OH group of iron-coordinated ethanol and the terminal chloride ligands of Ru (Fig. 3). Complex **5** has two structural isomers: a linear one (**5**) and a bent one (**5b**, and **5c**) (Fig. 5).

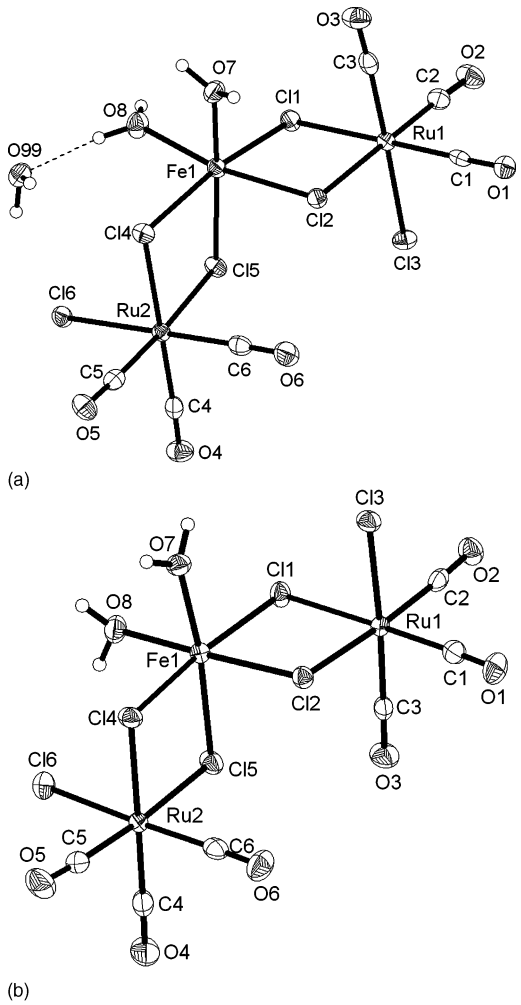

Fig. 5 (a): Thermal ellipsoid plot (50% probability level) of the bent $[Ru_2Cl_2(\mu\text{-}Cl)_4(CO)_6Fe(H_2O)_2]\cdot(H_2O)$ (**5b**). Hydrogen bonding: O8–H8B: 0.85 Å, H(B···O99: 2.01(2) Å, O8···O99: 2.779(4) Å, O8–H8B···O99: 151(4)°. (b): Thermal ellipsoid (50% probability level) plot of the bent $[Ru_2Cl_2(\mu\text{-}Cl)_4(CO)_6Fe(H_2O)_2]$ (**5c**).

In most reactions the linear **5** was preferred over the bent **5b** one. However, the use of pure iron surfaces and, in particular, powdered iron increased the amount of bent **5b**. As shown in Fig. 4, the structure of linear **5** resembles closely that of **4** (Fig. 3). The linear arrangement is again supported by two intramolecular hydrogen bonds between the iron-bound water and the ruthenium coordinated chloride. In the isomer **5b** the crystal structure contains water of crystallization, which is involved in the hydrogen bonding network and may thus support the bent arrangement in preference to the linear one. However, the water of crystallization is not the key to the bent structure. A stable bent molecule without water of crystallization (**5c**) was also found, isolated, and crystallized (Fig. 5(b)). In the case of the bent **5b** and **5c**, the bent structure, together with very weak intramolecular hydrogen interactions, permitted some variations in the orientation of the end groups $[RuCl_3(CO)_3]$. We compared the relative stabilities of the linear and bent isomers of **5** and **5c** (or **5b**) by means of DFT calculations in the gas phase (Scheme 1). The calculations suggested that, energetically, the isomers are almost identical. The energy of the bent **5b** is only 4 kJ mol^{-1} lower than the corresponding value for the linear **5**. It can therefore be expected that there is no energetic preference in the formation of either structural form, and isomerization from one form to another may be possible.

3.2 Formation of the products

The formation of the aqueous products $[Fe(H_2O)_6]^{2+}$, $[FeCl_2(H_2O)]$, and $[RuCl_2(H_2O)(CO)_3]$ could be explained in terms of the simple oxidation of the iron surface during the partial reductive carbonylation of $RuCl_3$. Carbon monoxide facilitates the reaction further and stabilizes the ruthenium species. In such a mechanism, an iron-containing surface acts as a sacrificial surface, supplying iron ions to the solution. The corrosion of the metal is enhanced by the chlorides from $RuCl_3$, especially when stainless steel with a protective oxide layer on its surface is used. It is known that chloride and other aggressive anions can penetrate through the oxide layer into the metal surface and launch the corrosion process.[52] The corrosion products tend to be deposited on the metal surface, but as chloride also passes through the oxide layer it can also penetrate through the corrosion deposit, thus accelerating the corrosion even further. However, in the reduction conditions that we used, the reduction of ruthenium also accelerates the release of iron. This was seen clearly when the stainless steel surfaces were exposed to an ethanol solution of NaCl under CO pressure (50 bar) without Ru^{3+} ions. The extent of the corrosion was insignificant even after 20 h of reaction at 125 °C.

The formation of trinuclear complexes **4** and **5** is less obvious. A reaction between the released Fe^{2+} ions and the partially reduced ruthenium species would provide the most straightforward reaction route. If this was in fact the mechanism, it should be possible to obtain **4** and **5** simply by adding Fe^{2+} ions to the reaction solution. In order to investigate this possibility, the reductive carbonylation of $RuCl_3$ was repeated (at 125 °C, 20 bar, 3 h) by using dissolved $FeCl_2\cdot n(H_2O)$ as the iron source, instead of a metal surface. None of the reactions with dissolved $FeCl_2\cdot n(H_2O)$ produced **4** or **5**. The only Fe(II)-containing species found were *trans*(Cl)-$[FeCl_2(H_2O)_4]$ (**2**) and ionic **1**. In addition to the Fe(II) products, traces of a further oxidized iron(III) component, $[RuCl_3(CO)_3][FeCl_2(H_2O)_4]\cdot 2(H_2O)$ (**6**), was also found. The Fe^{3+} product **6** was crystallized and characterized by X-ray diffraction (Fig. 6). No other Fe^{3+} products were found in any of the reactions. In reactions with metal surfaces the oxidation of the iron stopped at oxidation state +2 and no **6** was observed. If **4** and **5** are formed in solution as a result of a reaction between the dissolved Fe^{2+} species **1** or **2** and the ruthenium species, the extended reaction should eventually consume the mononuclear iron and ruthenium components, thus improving the yields of **4** and **5**, but this was not observed. Such results may indicate a more

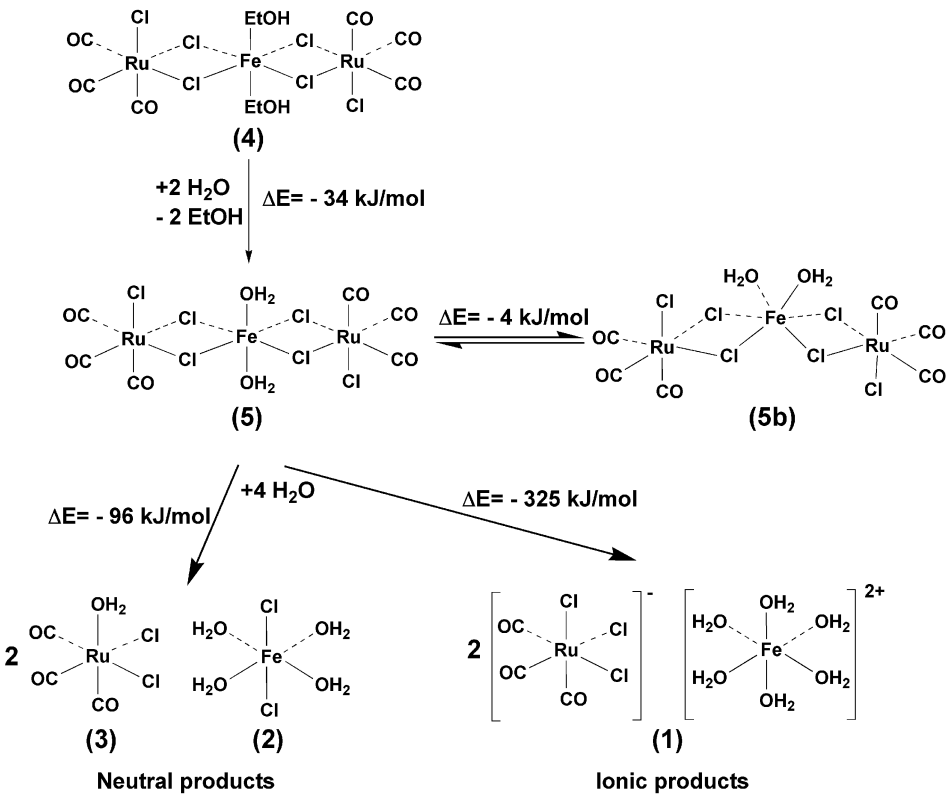

Scheme 1

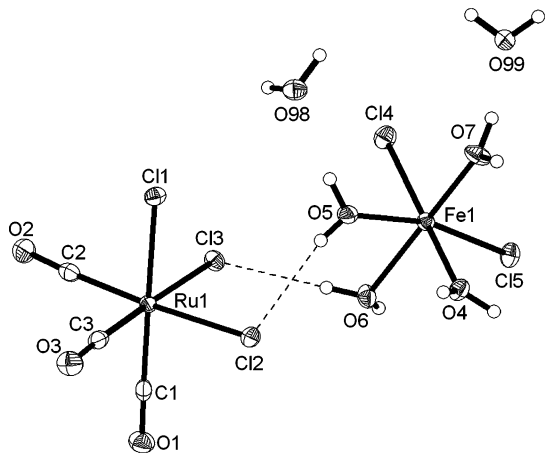

Fig. 6 Thermal ellipsoid plot of $[RuCl_3(CO)_3][FeCl_2(H_2O)_4]\cdot 2(H_2O)$ (**6**). The ellipsoids have been drawn at 50% probability level. Intermolecular hydrogen bonding interactions: O5–H5B: 0.77 Å, H5B · · · Cl2: 2.40 Å, O5 · · · Cl2: 3.158(2) Å, O5–H5B · · · Cl2: 170.4°, O6–H6A: 0.82 Å, H6A · · · Cl3: 2.33 Å, O6 · · · Cl3: 3.151(2) Å, O6–H6A · · · Cl3: 178.2°.

active role for the metal surface, for example, in the surface-assisted formation of **4** and **5**.

The energetics of the interconversions between products **1–5** was investigated using computational DFT methods. The results are summarized in Scheme 1.

The DFT calculations predict that the reaction of **4** with water (Scheme 1) leads to the replacement of the ethanol ligands by water. The total energy difference of −34 kJ^{-1} mol for the replacement reaction is not large, but it is favorable. According to the calculations, the presence of water should thus favor **5** over **4**. In addition, both the linear and the bent isomers **5** and **5b** should be more or less equally probable products. It should be noted that the gas phase calculations tend to overestimate the role of the intramolecular hydrogen bonds, and therefore the stability of **4** and **5**, as a result of the absence of surrounding solvent and molecules. However, both **4** and **5** contain intramolecular hydrogen bonds, which should make the calculations more compatible when **4** and **5** are compared.

According to the DFT results, the amount of water is one of the key factors determining the distribution of the products. A suitable amount of water should favor **4**, but an excess leads to a breakdown of the trinuclear framework of the $[Ru_2Cl_2(\mu\text{-}Cl)_4(CO)_6Fe(H_2O)_2]$ into mononuclear products, either as ionic $[RuCl_3(CO)_3]_2[Fe(H_2O)_6]$ (**1**) or as a mixture of neutral $FeCl_2(H_2O)_4$ (**2**) and $RuCl_2(H_2O)(CO)_3$ (**3**). Both fragmentation reactions $[Ru_2Cl_2(\mu\text{-}Cl)_4(CO)_6Fe(H_2O)_2] + 4\ (H_2O) \rightarrow [RuCl_3(CO)_3]_2[Fe(H_2O)_6]$ and $[Ru_2Cl_2(\mu\text{-}Cl)_4(CO)_6Fe(H_2O)_2] + 4\ (H_2O) \rightarrow 2\ RuCl_2(H_2O)(CO)_3 + FeCl_2(H_2O)_4$ are favorable (Scheme 1), but the ionic products should clearly be more likely than the neutral products. Again, the absolute energy values obtained from the gas phase calculations should be interpreted with caution, especially in the case of the ionic products. The gas phase optimization overestimates the hydrogen bonding interactions between $[RuCl_3(CO)_3]^-$ and $[Fe(H_2O)_6]^{2+}$ and therefore the stability of $[RuCl_3(CO)_3]_2[Fe(H_2O)_6]$ is also overestimated. Nevertheless, the breakdown of **4** to **1** is so facile that the calculations can be expected to give the right results on at least

a qualitative level. Furthermore, computational results strongly support the experimental observations: the main product in all short (3 h) low pressure (10 bar) reactions is ionic **1**, and only small amounts, if any, of the neutral $RuCl_2(H_2O)(CO)_3$ (**2**) and $FeCl_2(H_2O)_4$ are formed. Furthermore, when water was added to the reaction solution, products **4** or **5** were no longer obtained, and only aqueous mononuclear metal species **1–3** were found. In addition, the fact that the reaction time does not favor the formation of **4** or **5** is in agreement with the calculations. It seems very unlikely that the trinuclear **4** or **5** are formed in a reaction between **1–3**. This may therefore mean that the presence of a metal surface is required to obtain these rather labile complexes. Most probably, there is a more straightforward reaction pathway to **1–3**, but the breaking down of the trinuclear complexes certainly offers a facile route to these species.

Formation of **4** and **5** shows that the sacrificial surface approach can be used for the synthesis of new mixed metal Ru–Fe compounds. The oxidation process is driven by the potential differences between the Ru^{3+} ions and the Fe surface. This method can also be expanded to other metals. We are currently working with Ru–Co, Os–Fe and Os–Co systems. Scheme 1 also shows the main challenge involved in using the method: The mixed metal compounds are relatively labile and sensitive to moisture, which causes problems in the reproducibility of compounds **4** and **5**. The sensitivity of moisture is also the main reason for variations in the product distributions.

4. Conclusions

An iron-containing metal surface can act as a sacrificial source for iron in the synthesis of mixed metal $[Ru_2Cl_2(\mu\text{-}Cl)_4(CO)_6Fe(L)_2]$ compounds. The carbonylative reduction of Ru(III) promotes the oxidation of the iron to Fe(II), which in turn leads to the release of iron species from the surface. The oxidized iron component can be exploited in the synthesis of labile trinuclear mixed metal products. Thus, the use of active solid-metal surfaces offers a new route to a series of oligonuclear and multinuclear mixed metal complexes.

Acknowledgements

Financial support in the form of a grant (grant no. 210265) provided by the Academy of Finland is gratefully acknowledged. The authors would also like to thank Dr Janne Jänis for his help and valuable comments.

Notes and references

1 See for example: (*a*) A. N. Nesmeyanov, R. Kh. Freidlina, E. Ts. Chukovskaya, R. G. Petrova and A. B. Belyaskii, *Tetrahedron*, 1962, **17**, 61; (*b*) V. N. Ipatieff, H. Pines and E. E. Meisinger, *J. Am. Chem. Soc.*, 1949, **71**, 2934; (*c*) H. I. Waterman and C. van Vlodrop, *Recl. Trav. Chim. Pays-Bas*, 1933, **52**, 469.
2 D. P. Siegwarth and R. J. Law, *Eur. Pat.*, 1403881, 2004.
3 D. R. Colledge and C. McKechie, *World Pat.*, 03031344, 2003.
4 V. N. E. Robinson, *World Pat.*, 0168532, 2001.
5 M. Kobya, O. Taner and M. Bayramoglu, *J. Hazard. Mater.*, 2003, **B100**, 163.
6 D. G. Braithwaite, J. S. D'Amico, P. L. Gross and W. Hanzel, *US Pat.*, 3141841, 1964.
7 C. Gosmini, J. Y. Nédélec and J. Périchon, *Tetrahedron Lett.*, 2000, **41**, 5039.
8 H. Fillon, C. Gosmini, J. Y. Nédélec and J. Périchon, *Tetrahedron Lett.*, 2001, **42**, 3843.
9 D. A. Garnovskii, M. F. C. Guedes da Silva, M. N. Kopylovich, A. D. Garnovskii, J. R. R. Fraústo da Silva and A. J. L. Pombeiro, *Polyhedron*, 2003, **22**, 1335.
10 J. Chatt, B. L. Shaw and A. E. Field, *J. Chem. Soc.*, 1964, 3466.
11 J. M. Kelly, C. M. O'Connell and J. G. Vos, *Inorg. Chim. Acta*, 1982, **64**, L75.
12 A. Mantovani and S. Cenini, *Inorg. Synth.*, 1976, **16**, 47.
13 M. Fauré, L. Maurette, B. Donnadieu and G. Lavigne, *Angew. Chem., Int. Ed.*, 1999, **38**, 518.
14 M. Fauré, C. Saccavini and G. Lavigne, *Chem. Commun.*, 2003, 1578.
15 C. R. Eady, P. F. Jackson, B. F. G. Johnson, J. Lewis, M. C. Malatesta, M. McPartlin and W. J. H. Nelson, *J. Chem. Soc., Dalton Trans.*, 1980, 383.
16 M. I. Bruce and F. G. A. Stone, *J. Chem. Soc. A*, 1967, 1238.
17 M. L. Berch and A. Davidson, *J. Inorg. Nucl. Chem.*, 1973, **35**, 3763.
18 A. J. Deeming and M. Karim, *Polyhedron*, 1999, **10**, 837.
19 M. I. Bruce, C. M. Jensen and N. L. Jones, *Inorg. Synth.*, 1989, **26**, 259.
20 C. Roveda, E. Cariati, E. Lucenti and D. Roberto, *J. Organomet. Chem.*, 1999, **580**, 117.
21 L. Maurette, B. Donnadieu and G. Lavigne, *Angew. Chem., Int. Ed.*, 1999, **38**, 3707.
22 G. Lavigne, *Eur. J. Inorg. Chem.*, 1999, 917.
23 E. Lucenti, E. Cariati, C. Dragonetti and D. Roberto, *J. Organomet. Chem.*, 2003, **669**, 44.
24 H. A. Mirza, J. J. Vittal and R. J. Puddephatt, *Inorg. Chem.*, 1993, **32**, 1327.
25 D. Roberto, E. Cariati, R. Psaro and R. Ugo, *Organometallics*, 1994, **13**, 734.
26 D. Roberto, E. Cariati, E. Lucenti, M. Respini and R. Ugo, *Organometallics*, 1997, **16**, 4531.
27 E. Cariati, D. Roberto and R. Ugo, *Chem. Rev.*, 2003, **103**, 3707.
28 D. Roberto, R. Psaro and R. Ugo, *Organometallics*, 1993, **12**, 2292.
29 M. J. Cleare and W. P. Griffith, *J. Chem. Soc. A*, 1969, 372.
30 P. Hirva, M. Haukka, M. Jakonen and T. A. Pakkanen, *Inorg. Chim. Acta*, 2006, **359**, 853.
31 Z. Otwinowski and W. Minor, *Methods Enzymol.*, 1997, **276**, 307.
32 G. M. Sheldrick, *SHELXS97*, University of Göttingen, Göttingen, Germany, 1997.
33 M. C. Burla, R. Caliandro, M. Camalli, B. Carrozzini, G. L. Cascarano, L. De Caro, C. Giacovazzo, G. Polidori and R. J. Spagna, *Appl. Crystallogr.*, 2005, **38**, 381.
34 A. Altomare, M. C. Burla, M. Camalli, G. L. Cascarano, C. Giacovazzo, A. Guagliardi, A. G. G. Moliterni, G. Polidori and R. J. Spagna, *Appl. Crystallogr.*, 1999, **32**, 115.
35 L. J. Farrugia, *J. Appl. Crystallogr.*, 1999, **32**, 837.
36 G. M. Sheldrick, *SHELXTL, version 6.14-1*, Bruker AXS, Inc., Madison, WI, 2005.
37 G. M. Sheldrick, *SHELXL97*, University of Göttingen, Göttingen, Germany, 1997.
38 J. Meunier-Piret and M. van Meerssche, *Acta Crystallogr., Sect. B*, 1971, **27**, 2329.
39 J. J. Verbist, W. C. Hamilton, T. F. Koetzle and M. S. Lehmann, *J. Chem. Phys.*, 1972, **56**, 3257.
40 J. J. Bergmeister, III, B. E. Hanson and J. S. Merola, *Inorg. Chem.*, 1990, **29**, 4831.
41 M. Taimisto, R. Oilukaniemi, R. S. Laitinen and M. Ahlgrén, *Inorg. Chim. Acta*, 2003, **58**, 959.
42 M. J. Frisch, G. W. Trucks, H. B. Schlegel, G. E. Scuseria, M. A. Robb, J. R. Cheeseman, J. A. Montgomery, Jr., T. Vreven, K. N. Kudin, J. C. Burant, J. M. Millam, S. S. Iyengar, J. Tomasi, V. Barone, B. Mennucci, M. Cossi, G. Scalmani, N. Rega, G. A. Petersson, H. Nakatsuji, M. Hada, M. Ehara, K. Toyota, R. Fukuda, J. Hasegawa, M. Ishida, T. Nakajima, Y. Honda, O. Kitao, H. Nakai, M. Klene, X. Li, J. E. Knox, H. P. Hratchian, J. B. Cross, V. Bakken, C. Adamo, J. Jaramillo, R. Gomperts, R. E. Stratmann, O. Yazyev, A. J. Austin, R. Cammi, C. Pomelli, J. Ochterski, P. Y. Ayala, K. Morokuma, G. A. Voth, P. Salvador, J. J. Dannenberg, V. G. Zakrzewski, S. Dapprich, A. D. Daniels, M. C. Strain, O. Farkas, D. K. Malick, A. D. Rabuck, K. Raghavachari, J. B. Foresman, J. V. Ortiz, Q. Cui, A. G. Baboul, S. Clifford, J. Cioslowski, B. B. Stefanov, G. Liu, A. Liashenko, P. Piskorz, I. Komaromi, R. L. Martin, D. J. Fox, T. Keith, M. A. Al-Laham, C. Y. Peng, A. Nanayakkara, M. Challacombe, P. M. W. Gill, B. G. Johnson,

W. Chen, M. W. Wong, C. Gonzalez and J. A. Pople, *GAUSSIAN 03 (Revision C.02)*, Gaussian, Inc., Wallingford, CT, 2004.
43 The basis set was obtained from the Extensible Computational Chemistry Environment Basis Set Database, Version 9/12/01, as developed and distributed by the Molecular Science Computing Facility, Environmental and Molecular Sciences Laboratory, which is part of the Pacific Northwest Laboratory, P.O. Box 999, Richland, Washington 99352, USA, and funded by the U.S. Department of Energy. The Pacific Northwest Laboratory is a multi-program laboratory operated by the Battelle Memorial Institute for the U.S. Department of Energy under contract DE-AC06-76RLO 1830. Contact David Feller or Karen Schuchardt for further information.
44 *Gaussian Basis Sets for Molecular Calculations, Physical Sciences Data 16*, ed. S. Huzinaga, Elsevier, Amsterdam, 1984.
45 R. H. Crabtree, *The Organometallic Chemistry of the Transition Metals*, John Wiley & Sons, New York, 2nd edn, 1994, p. 260.
46 Y. Zhu, M. O. Wolf and G. P. A. Yap, *Inorg. Chem.*, 1997, **36**, 5483.
47 A. Bino and F. A. Cotton, *J. Am. Chem. Soc.*, 1980, **102**, 608.
48 F. A. Cotton and R. C. Torralba, *Inorg. Chem.*, 1989, **28**, 1516.
49 F. A. Cotton and R. C. Torralba, *Inorg. Chem.*, 1991, **30**, 3292.
50 F. A. Cotton and R. C. Torralba, *Inorg. Chem.*, 1991, **30**, 4386.
51 R. Goerissen, U. Koelle and T. P. Spaniol, *Polyhedron*, 1992, **11**, 2317.
52 H.-H. Strehblow, in *Corrosion Mechanism in Theory and Practice*, ed. P. Marcus, Marcel Dekker, New York, 2nd edn, 2002, p. 243.

